

# Terahertz probe for spectroscopy of sub-wavelength objects

Oleg Mitrofanov,\* Cyril C. Renaud, and Alwyn J. Seeds

Department of Electronic & Electrical Engineering, University College London, Torrington Place, London, WC1E 7JE, UK

\*o.mitrofanov@ucl.ac.uk

**Abstract:** A system of two probes is designed for terahertz (THz) time-domain spectroscopy of sub-wavelength size objects. A twin-needle probe confines broadband THz pulses spatially by means of surface plasmon waves to a sub-wavelength spot smaller than 10 microns. The confined pulses are detected within the near-field zone of the twin-needle probe by a sub-wavelength aperture probe. The system allows THz spectroscopy to be applied to single micrometer-size objects in the 1-2.5THz region.

©2012 Optical Society of America

**OCIS codes:** (300.6495) Terahertz spectroscopy; (180.4243) Near-field microscopy; (110.6795) Terahertz imaging; (240.6680) Surface plasmons; (320.7100) Ultrafast measurements.

---

## References and links

1. R. Ulbricht, E. Hendry, J. Shan, T. Heinz, and M. Bonn, "Carrier dynamics in semiconductors studied with time-resolved terahertz spectroscopy," *Rev. Mod. Phys.* **83**(2), 543–586 (2011).
2. A. Dienst, M. C. Hoffmann, D. Fausti, J. C. Petersen, S. Pyon, T. Takayama, H. Takagi, and A. Cavalleri, "Bi-directional ultrafast electric-field gating of interlayer charge transport in a cuprate superconductor," *Nat. Photonics* **5**(8), 485–488 (2011).
3. T. M. Korter, R. Balu, M. B. Campbell, M. C. Beard, S. K. Gregurick, and E. J. Heilweil, "Terahertz spectroscopy of solid serine and cysteine," *Chem. Phys. Lett.* **418**(1-3), 65–70 (2006).
4. R. A. Kaindl, M. A. Carnahan, D. Hägele, R. Lövenich, and D. S. Chemla, "Ultrafast terahertz probes of transient conducting and insulating phases in an electron-hole gas," *Nature* **423**(6941), 734–738 (2003).
5. O. Mitrofanov, M. Lee, J. W. P. Hsu, I. Brener, R. Harel, J. F. Federici, J. D. Wynn, L. N. Pfeiffer, and K. W. West, "Collection-mode near-field imaging with 0.5-THz pulses," *IEEE J. Sel. Top. Quantum Electron.* **7**(4), 600–607 (2001).
6. J. Zhu, S. K. Ozdemir, Y.-F. Xiao, L. Li, L. He, D.-R. Chen, and L. Yang, "On-chip single nanoparticle detection and sizing by mode splitting in an ultrahigh-Q microresonator," *Nat. Photonics* **4**(1), 46–49 (2010).
7. V. Astley, B. McCracken, R. Mendis, and D. M. Mittleman, "Analysis of rectangular resonant cavities in terahertz parallel-plate waveguides," *Opt. Lett.* **36**(8), 1452–1454 (2011).
8. M. Schnell, P. Alonso-González, L. Arzubia, F. Casanova, L. E. Hueso, A. Chuvilin, and R. Hillenbrand, "Nanofocusing of mid-infrared energy with tapered transmission lines," *Nat. Photonics* **5**(5), 283–287 (2011).
9. H. Zhan, R. Mendis, and D. M. Mittleman, "Superfocusing terahertz waves below  $\lambda/250$  using plasmonic parallel-plate waveguides," *Opt. Express* **18**(9), 9643–9650 (2010).
10. M. A. Seo, H. R. Park, S. M. Koo, D. J. Park, J. H. Kang, O. K. Suwal, S. S. Choi, P. C. M. Planken, G. S. Park, N. K. Park, Q. H. Park, and D. S. Kim, "Terahertz field enhancement by a metallic nano slit operating beyond the skin-depth limit," *Nat. Photonics* **3**(3), 152–156 (2009).
11. R. D. Grober, R. J. Schoelkopf, and D. E. Prober, "Optical antenna: Towards a unity efficiency near-field optical probe," *Appl. Phys. Lett.* **70**(11), 1354–1356 (1997).
12. R. Mendis and D. Grischkowsky, "Undistorted guided-wave propagation of subpicosecond terahertz pulses," *Opt. Lett.* **26**(11), 846–848 (2001).
13. M. Mbyone, R. Mendis, and D. M. Mittleman, "A terahertz two-wire waveguide with low bending loss," *Appl. Phys. Lett.* **95**(23), 233506 (2009).
14. M. Theuer, R. Beigang, and D. Grischkowsky, "Sensitivity increase for coating thickness determination using THz waveguides," *Opt. Express* **18**(11), 11456–11463 (2010).
15. P. C. M. Planken and N. C. van der Valk, "Spot-size reduction in terahertz apertureless near-field imaging," *Opt. Lett.* **29**(19), 2306–2308 (2004).
16. A. J. Huber, F. Keilmann, J. Wittborn, J. Aizpurua, and R. Hillenbrand, "Terahertz near-field nanoscopy of mobile carriers in single semiconductor nanodevices," *Nano Lett.* **8**(11), 3766–3770 (2008).
17. K. Ishihara, K. Ohashi, T. Ikari, H. Minamide, H. Yokoyama, J. Shikata, and H. Ito, "Terahertz-wave near-field imaging with subwavelength resolution using surface-wave-assisted bow-tie aperture," *Appl. Phys. Lett.* **89**(20), 201120 (2006).

18. A. Rusina, M. Durach, K. A. Nelson, and M. I. Stockman, "Nanoccentration of terahertz radiation in plasmonic waveguides," *Opt. Express* **16**(23), 18576–18589 (2008).
19. R. Mueckstein and O. Mitrofanov, "Imaging of terahertz surface plasmon waves excited on a gold surface by a focused beam," *Opt. Express* **19**(4), 3212–3217 (2011).
20. R. Mueckstein, C. Graham, C. C. Renaud, J. A. Seeds, J. A. Harrington, and O. Mitrofanov, "Imaging and analysis of THz surface plasmon polariton waves with the integrated sub-wavelength aperture probe," *J. Infrared Millim. THz Waves* **32**(8–9), 1031–1042 (2011).
21. O. Mitrofanov and J. A. Harrington, "Dielectric-lined cylindrical metallic THz waveguides: mode structure and dispersion," *Opt. Express* **18**(3), 1898–1903 (2010).
22. K. Wang and D. M. Mittleman, "Metal wires for terahertz wave guiding," *Nature* **432**(7015), 376–379 (2004).
23. T. Jeon, J. Zhang, and D. Grischkowsky, "THz Sommerfeld wave propagation on a single metal wire," *Appl. Phys. Lett.* **86**(16), 161904 (2005).
24. M. Wächter, M. Nagel, and H. Kurz, "Frequency-dependent characterization of THz Sommerfeld wave propagation on single-wires," *Opt. Express* **13**(26), 10815–10822 (2005).
25. O. Mitrofanov, T. Tan, P. R. Mark, B. Bowden, and J. A. Harrington, "Waveguide mode imaging and dispersion analysis with terahertz near-field microscopy," *Appl. Phys. Lett.* **94**(17), 171104 (2009).
26. O. Mitrofanov, L. N. Pfeiffer, and K. W. West, "Generation of low-frequency components due to phase-amplitude modulation of subcycle far-infrared pulses in near-field diffraction," *Appl. Phys. Lett.* **81**(9), 1579–1581 (2002).
27. P. D. Cunningham and L. M. Hayden, "Optical properties of DAST in the THz range," *Opt. Express* **18**(23), 23620–23625 (2010).

---

## 1. Introduction

Unique spectroscopic signatures displayed by molecules, phonons and excitons in the terahertz (THz) frequency region enable direct and non-invasive probing of electronic states and chemical composition [1–4]. The THz signature of charge carriers in quantum wells, for example, allows distinguishing between the correlated and independent motion of electron-hole pairs [4]. However single nano- and micro-scale objects, such as quantum dots, nanowires, or cells, exhibit very weak interaction with THz radiation due to their sub-wavelength size. A system of two probes described here mitigates this problem: a twin-needle probe is employed to confine broadband THz pulses by means of surface plasmon waves to a sub-wavelength spot smaller than  $10\mu\text{m}$ , and a sub-wavelength aperture probe [5] is used to detect the confined field within the near-field zone.

According to electromagnetic wave theory, the wave energy cannot be focused in a homogeneous medium to a volume with dimensions smaller than approximately one half of the wavelength. Therefore only a small portion of the wave energy interacts with single sub-wavelength-size objects, even if the wave is focused down to the diffraction limit. If the full spectroscopic signature is not required, the weak coupling can be mitigated by the use of narrow band resonant structures, which increase the interaction between the wave and the object within narrow frequency bands [6,7]. To increase the interaction throughout a wide spectral range, the electromagnetic energy must be confined to a sub-wavelength-size volume.

The electromagnetic field can be bound by a metallic surface. Supported by the surface plasmon waves, the electromagnetic wave therefore can be confined between two isolated metallic surfaces to a volume significantly smaller than the wavelength [8–11], avoiding the frequency cutoff effect [12,13]. Wave confinement in the parallel plate configuration allowed the extension of THz spectroscopy to thin sub-wavelength films [14]. To achieve a higher degree of confinement, required for single sub-wavelength-size objects, metallic needles, microstrip waveguides, slits and tapered parallel plate waveguides have been studied [8–11,15–18].

The non-radiative nature of the confined wave makes the use of such structures with far-field detectors highly inefficient. To realize a system for spectroscopy of single sub-wavelength objects, here we combine the sub- $10\mu\text{m}$  confinement that we achieved using a twin-needle probe, with an integrated sub-wavelength aperture THz probe [5], which we position in the near-field region of the needle tips to detect the confined THz waves (Fig. 1(a)). When the aperture is aligned with the twin-needle probe (Fig. 1(a), inset) the photoconductive antenna below the aperture detects the electric field between the needle tips because the evanescent wave from the tips couples through the aperture and induces electric field in the antenna gap. The metallic screen on the surface of the integrated probe prevents

any incident wave from reaching the detector except for the wave confined by the twin-needle probe. Focused by the needles and detected in the near-field zone, the THz pulses preserve a wide bandwidth (1-2.5THz) and experience no noticeable dispersion, opening the door to THz spectroscopy of single micrometer-size objects. The structure of the twin-needle probe provides a convenient way to hold a micrometer-scale object in the region of field confinement for THz spectroscopy.

## 2. Wave confinement by the twin-needle probe

The twin-needle probe is designed to couple an incident electromagnetic wave into a surface wave, which is then guided along two 0.5mm diameter PtIr needles towards their tips (Fig. 1(a)). The needles have mechanically polished ends with tip radius of smaller than  $1\mu\text{m}$ . The probe is fabricated by manually aligning the two needles to form a gap of  $\sim 5\text{-}10\mu\text{m}$  between the tips. Both needles are in the  $xz$ -plane at the angles of 30 degrees with respect to the optical axis (Fig. 1(a,b)). The needles are mounted on a rigid holder (Fig. 1(b)) in order to keep the relative position of the needles constant. The holder is attached to a motorized  $xyz$ -translation stage, which allows precise positioning of the twin-needle probe with respect to the integrated aperture probe.

To confirm the operation principle, the field distribution near the needles is investigated first on a large scale, using the sub-wavelength aperture probe, which is sensitive to both the incident transverse waves and the surface waves [19,20]. In the experiment, the incident THz beam is formed by a dielectric-lined hollow metallic waveguide [21], which produces an unfocused wave with a circular spatial profile and a flat wave front (Fig. 1(c,d), left panels). The incident wave is  $x$ -polarized for optimal coupling to the surface wave in the twin-needle probe. The sub-wavelength aperture probe contains a low-temperature grown GaAs photoconductive antenna [5], which is also oriented along the  $x$ -axis for maximal sensitivity. The integrated probe is built on a sapphire substrate to allow optical access to the antenna.

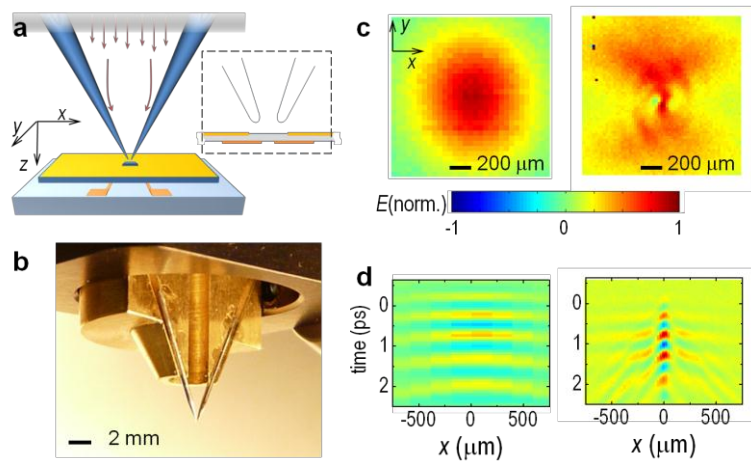


Fig. 1. Twin-needle probe system for THz spectroscopy. (a) Schematic diagram of the probe positioned above the aperture of the integrated near-field probe. The THz pulse is incident from above (indicated by red arrows). Inset: cross section of the system showing the needle tips, the aperture in the gold screen and the photoconductive antenna. (b) Optical image of the twin-needle probe. (c) Electric field distribution of the incident THz pulse (left) and the field distribution near the twin-needle probe (right). (d) Space-time maps of the incident THz pulse (left) and the pulse focused by the twin-needle probe (right). To show the field enhancement both space-time maps are normalized to the maximal amplitude for the twin-needle probe.

The twin-needle probe changes the uniform field distribution and creates a point of enhanced electric field near the needle tips (Fig. 1(c,d), right panels). The spatial profile also displays two triangular shadows, produced by the needles blocking the wave from reaching the aperture probe directly, and fringes within the shadow regions.

The fringes represent an instantaneous image of the surface waves that couple from the tips to the metallic surface of the detector probe. Consider a space-time map measured along the  $x$ -axis passing through a point where the twin-needle probe is centered (Fig. 1(d), right panel). Three types of waves can be distinguished: the incident wave that displays a broad flat wave front similar to the left panel, the focused surface wave between the needles (near  $x = 0$ ), and the surface waves that appear ‘tilted’ in the space-time map. The tilted signature is typical for the surface waves that move along the gold surface of the sub-wavelength aperture probe [19,20]. These results show that the incident THz pulse excites surface (Sommerfeld) waves [13,22–24] travelling along the needles towards the tips. The THz wave is confined and enhanced in the region of the shortest distance between the needle tips.

To determine the degree of field confinement we map the electric field distribution using a high-resolution near-field probe with a  $10\mu\text{m}$  aperture positioned at  $z_0$  ( $\sim 1\text{--}2\mu\text{m}$  from the tips). Figure 2(a) shows a  $100\times 100\mu\text{m}^2$  region, where a bright area corresponds to the region of enhanced electric field between the needle tips. The needles ‘cast’ triangular shadows to the right and to the left of the bright area. Figure 2(b) shows linear scans along the  $x$ -axis. Both scans (marked as A and B and separated by  $\Delta y = 2.5\mu\text{m}$ ) pass through the area of enhanced field and show the intensity profile with the full width at half maximum (FWHM) of  $9\mu\text{m}$ . The region of field confinement can be smaller however the spatial resolution of the  $10\mu\text{m}$  aperture probe prevents the observation of finer details.

The wave experiences weaker focusing along the  $y$ -axis. The shape of the vertical line scan (C) shows a narrow region of enhanced field with a FWHM of  $15\mu\text{m}$  rising over a broader region. The latter has an elliptical shape in Fig. 2(a), similar to the diffraction pattern formed by the incident wave. The image therefore shows a superposition of the confined surface wave and the diffracted wave. The field confinement region is smaller than  $9\times 15\mu\text{m}$ , similar to the smallest spot sizes that have been demonstrated with THz pulses [9,15].

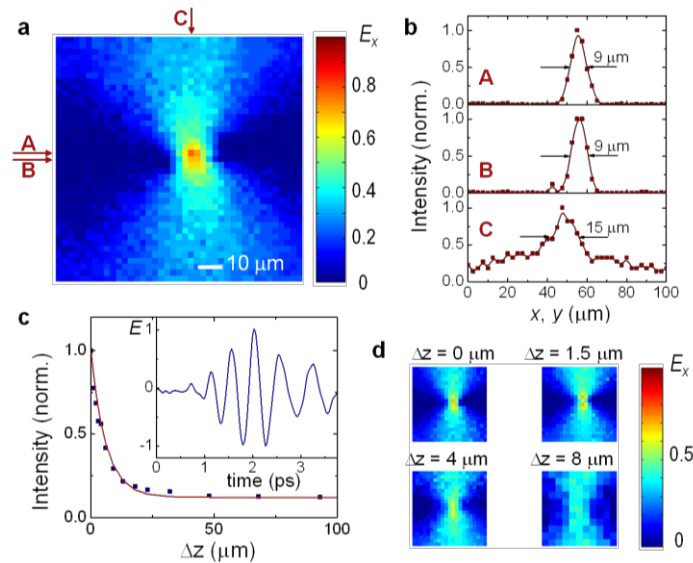


Fig. 2. Confinement of the THz wave by the twin-needle probe. (a) High-resolution  $100\times 100\mu\text{m}$  map of the electric field confined by the needles. (b) Linear scans of  $E^2$  along the  $x$ - and  $y$ -direction passing through the focus. (c)  $z$ -dependence of the time-integrated intensity of the confined THz field. Inset: waveform of the confined THz pulse. (d) Electric field distributions in the same area as in (a) at a larger distance  $z_0 + \Delta z$  from the needle tips.

The sub-wavelength confinement in the  $xy$ -plane makes the field non-radiative, i.e. the focused wave can extend past the tip of the needle-probe only as an evanescent wave. To determine the confinement in the  $z$ -direction, the near-field detector is positioned in the centre of the confined region and the THz pulse waveforms are measured while the twin-needle

probe is moved away from the detector. The field strength decreases quickly with the distance from the tip, down to the level of the incident wave amplitude. The time-averaged intensity of the detected THz pulse shown in Fig. 2(c) follows an exponential decay with the characteristic length of  $6\mu\text{m}$ . The vertical offset of the intensity data is due to the incident plane wave, which continues propagating in the  $z$ -direction after diffracting on the needles.

It is important to note that the diffracted wave that can be detected in the far-field, would be practically unaffected by an object placed between the needles. The diffracted wave is determined primarily by the macroscopic shape of the needles, rather than the field near the tips. A series of two-dimensional images measured at different positions  $z$  (Fig. 2(d)) shows how the bright spot, which corresponds to the enhanced field between the needles, fades as the distance between the needle probe and the aperture probe  $z_0 + \Delta z$  increases, leaving only the diffracted wave in the image. To perform spectroscopy of an object positioned between the needles, it is therefore essential to detect the field within the decay length shown in Fig. 2(c).

### 3. Frequency response of the twin-needle probe

For spectroscopy applications, the spectral response of the twin-needle probe is as important as the field confinement. The coupling of the incident THz pulses into the surface waves and their propagation along the needles imposes no significant effect on the waveform of the THz pulse. The twin-needle configuration exhibits no resonant response and no dispersion and therefore it is ideal for broadband THz spectroscopy. For precise characterization of the spectral response, we used a system of two parabolic (P1 and P4) and flat (M2 and M3) mirrors shown in Fig. 3(a) to direct the THz beam to the twin-needle probe, with the tip aligned directly above the sub-wavelength aperture probe. This system is chosen over the waveguide system in Fig. 1(a) because spectroscopic artefacts can be caused by the interference between waveguide modes [25]. The coupling efficiency between the waveguide and the twin-needle probe, and propagation losses along the needles are mode-dependent. Therefore, if in addition to the dominant  $\text{HE}_{11}$  mode, higher order modes (e.g.  $\text{HE}_{12}$  or  $\text{TE}_{01}$ ) are present in the waveguide [21], the measured spectral response of the probe ( $E_{\text{probe}}/E_{\text{inc}}$ ) is an average over the incident modes.

The spectral amplitude of the pulse confined between the needles is compared to the incident THz pulse. The field amplitude of the confined wave is stronger throughout the whole available frequency range. The amplitude ratio, which represents the frequency response of the twin-needle probe, however shows that the enhancement is larger at lower frequencies (Fig. 3(b)). The amplitude loss follows the  $f^{1/2}$ -dependence (dashed line) and it is therefore attributed to the Ohmic losses experienced by the THz surface waves [23,24].

To evaluate the potential of the complete system for THz spectroscopy, the frequency response of the sub-wavelength aperture probe also must be considered. The response is a product of the photoconductive antenna response, determined by the photocarrier lifetime, and the transmission spectrum of the sub-wavelength aperture (the transmitted amplitude increases with frequency linearly (Fig. 3(b)) [26]). The overall sensitivity is therefore limited due to the reduced transmission through the aperture at low frequencies and due to the Ohmic losses on the needle surfaces and the photoconductive antenna response at high frequencies.

The complete system allows detection of THz pulses within the frequency spectrum from 1 to 2.5 THz (Fig. 3(c)). The detected spectrum (inset) clearly resolves atmospheric absorption lines (e.g. 1.41, 1.69, and 1.73THz) due to propagation of the pulse through air (19 cm at 50% RH). If we now suppose that a  $10\mu\text{m}$  diameter object is placed between the needles, e.g. a crystal of organic salt DAST, which has several narrow phonon resonance in the THz range [27], we find that the crystal should cause  $\sim 40\%$  reduction in the detected power at the resonant frequency. This level of absorption can be resolved with the present system.

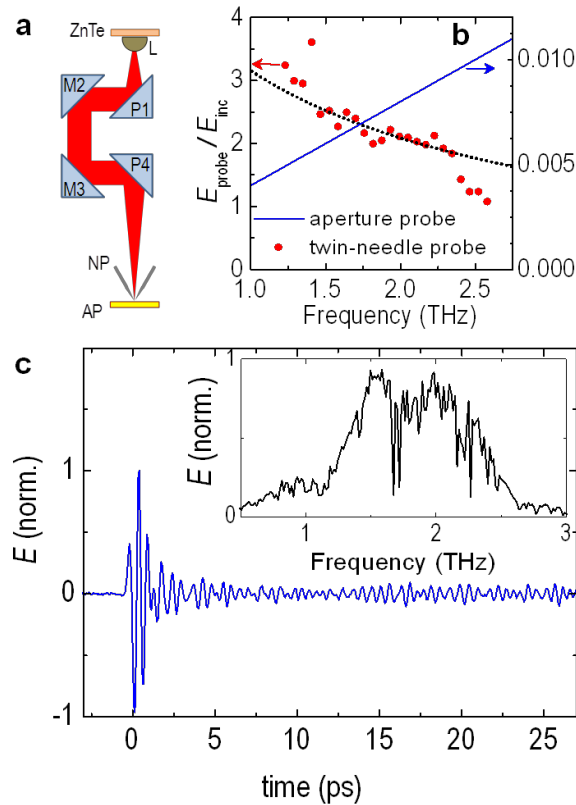


Fig. 3. Spectral response of the twin-needle probe. (a) Schematic diagram of the experimental setup. THz pulses are generated in a ZnTe crystal, focused by a system consisting of a Si lens (L), two parabolic mirrors (P1, P4) and two flat mirrors (M2, M3) in the region of the needle probe (NP), and detected by the sub-wavelength aperture probe (AP). (b) Spectral response of the twin-needle probe (red squares and dotted line) and transmission spectrum of the sub-wavelength aperture (blue line). (c) Waveform and spectrum (inset) of the detected THz pulse.

#### 4. Conclusion

The system of two probes described here opens the THz spectroscopy method to single sub-wavelength objects with volumes of only  $10^{-4}\lambda^3$ . The twin-needle probe also resolves the difficulty of holding and positioning of individual micrometer-size objects. The field confinement power of the probe is not limited to the level achieved here. Spatial modulation techniques can be applied to improve the system sensitivity and therefore can allow further confinement of THz pulses, possibly to the level of  $1\mu\text{m}$ .

#### Acknowledgment

The authors gratefully acknowledge J.A Harrington for providing the waveguide and C. F. Hirjibehedin and N.J. Curson for useful discussions. This work was supported by the Royal Society [grant number UF080745] and the Engineering and Physical Sciences Research Council [grant number EP/G033870/1].